Available online at www.sciencedirect.com
SCIENCE DIRECT®
Polymer 45 (2004) 3735–3746
polymer
www.elsevier.com/locate/polymer

Effect of clay type on morphology and thermal stability of PMMA–clay nanocomposites prepared by heterocoagulation method

Yijin Xu, William J. Brittain*, Chenchen Xue, Ronald K. Eby

Department of Polymer Science, The University of Akron, Akron, OH 44325-3909, USA

Received 3 March 2004; accepted 9 March 2004

Abstract

Poly(methyl methacrylate) (PMMA)–clay nanocomposites were prepared by a heterocoagulation method. A cationic PMMA emulsion was prepared by emulsion polymerization using a cationic initiator in the presence of free surfactant, cetyl trimethylammonium bromide (CTABr), followed by mixing with an aqueous clay slurry. Clays used in present research included montmorillonite (MMT), synthetic hectorites and fluorohectorites (with two different sizes). WAXD results and TEM images indicate that the morphologies of these nanocomposites depend on clay colloid stability as well as clay loadings. WAXD and TEM results also indicate the good morphology preservation of the nanocomposites during solution and melt processing. Thermal stability of these nanocomposites was studied by TG–DTG analyses; the mechanism of thermal stability improvement is discussed based on experimental results.

Keywords: Nanocomposites; Clay; Polyolefins

1. Introduction

Since the pioneering work of Toyota group on Nylon–clay nanocomposites [1], polymer-layered silicate nanocomposites (PLSNs) have generated considerable interest in both industrial and academic labs. Due to the molecular level interactions, nano-scale dimensions, and high aspect ratio of the silicate, many PLSNs show improvements in mechanical, electrical, optical, barrier, and thermal properties when compared with micro- and macro-composite counterparts [2].

In the study of thermoplastic–clay nanocomposites, poly(methyl methacrylate) (PMMA) and polystyrene (PS) have been widely used as a model polymer matrix because they can be easily polymerized by bulk, solution, suspension and emulsion techniques. In the preparation of PMMA–clay nanocomposites, many methods have been pursued to produce exfoliated structures including solution mixing [3], melt blending [4], and in situ polymerization (see below). Due to limited solvent matching of OLS (organically modified layered silicate) and polymer, the solution mixing method is limited to academic research. To get fully exfoliated polymer–clay nanocomposites with the second method, the clay and/or polymers must be first modified to increase the compatibility between them. Therefore, much research has been directed to in situ polymerization methods: bulk and solution in situ polymerization in the presence of organically modified clays [5], emulsion polymerization [5i,6] and suspension polymerization using pristine or organically modified clays [5i,6c]. Compatibility among modifier, monomer and initiator determines the structure (intercalated or exfoliated) of the nanocomposites in bulk and solution polymerization. Using pristine clay as a pickering co-emulsifier in emulsion polymerization only results in an intercalated morphology [6a]. The use of a cationic comonomer, which can exchange with the gallery cations, can give rise to a fully exfoliated structure [6b–d]. Using cationic comonomers in the preparation of exfoliated nanocomposites may result in crosslinking and thus leads to processing problems [7]. However, none of this cited research mentioned the processability of those nanocomposites. In a previous publication [6c], we reported a new method to prepare PMMA–clay nanocomposites by combination of conventional emulsion polymerization and subsequent cationic exchange reaction of the cationic emulsion with clay suspended in water. Although we used the term of 'emulsion

* Corresponding author. Fax: 1-330-972-5290.
E-mail address: wjbritt@uakron.edu (W.J. Brittain).

0032-3861/$ - see front matter © 2004 Elsevier Ltd. All rights reserved.
doi:10.1016/j.polymer.2004.03.058

polymerization' to describe this process in that paper; hereafter, we will name this process 'heterocoagulation method'.

The heterocoagulation method has been widely used in the preparation of nanocomposites: inorganic/inorganic, inorganic/organic, and organic/organic (here organic refers to polymer) [8]. Recently this method was also used to prepare polymer–clay nanocomposites [9,6c]. It is generally accepted that the morphology of (nano)composites by heterocoagulation process is controlled by surface charges, particle sizes, and particle number ratio (PNR). In the preparation of polymer–clay nanocomposites by this method, the surface charge of polymer latex and hence the electrostatic interaction between polymer latex particles and clay platelets determines the final morphology of nanocomposites; only cationic polymer latex–clay systems generated fully exfoliated polymer–clay nanocomposites [6c].

A major challenge in developing polymer–clay nanocomposites is to control morphology. We believe that the heterocoagulation method is a versatile method for preparing polymer–clay nanocomposites in systems, where the polymers can be radically polymerized.

Thermal stability is an important issue in PLSNs. It is generally accepted that the improvement in thermal stability is related to barrier properties and the radical-trapping effect of clay platelets. A few papers addressed the effect of special metal/metal oxide additives, but there are no systematic results to support their arguments [2a–c,10]. In this paper, we report the effect of clay dimensions on morphology and effect of clay chemical composition and dimension on the thermal stability of PMMA–clay nanocomposites

2. Experimental section

2.1. Materials

Montmorillonite (GelWhite GP® and Cloisite® Na^+) and (fluoro)hectorites (Laponite® RD, RDS, B, S, JS) were provided by Southern Clay Products. Synthetic fluorohectorite Somasif® ME100 was supplied by CO-OP Ltd., Japan. Information about CEC, dimensions and chemical compositions of these smectites are listed in Table 1. 2,2′-Azobis (2-amidinopropane) dihydrochloride (V-50), provided by Wako Pure Chemical Industries Ltd, was used without further purification. Cetyltrimethylammonium bromide (CTABr), tetrasodium pyrophosphate (TSPP) were obtained from Aldrich and used as received. Methyl methacrylate (MMA) from Aldrich was purified by distillation over CaH_2 before use. Deionized water was used in all the experiments.

2.2. Instrumentation

Wide angle X-ray diffraction (WAXD) results were obtained on a Rigaku diffractometer equipped with a rotating-anode generator system using Cu Kα radiation ($\lambda = 1.5418$ Å) at the scanning rate of 4°/min ranging from 1.5 to 10°; the operating current was 150 mA and voltage was 50 kV. Transmission electron microscopy (TEM) experiments were performed either on a JEM-1200EXII TEM at 60 kV accelerating voltage or on a TECNNAI TEM (FEI) at 120 kV accelerating voltage. The samples were ultra-microtomed with a diamond knife on a Reichert Ultracuts (Leica) microtome at room temperature to give ~50–70 nm thick sections. The sections were floated on water surface and collected with 300 mesh Cu grids. Thermogravimetric analysis (TGA) was performed on a

Table 1
Basic information about the smectites used in present paper

Name[a]	Abbreviation in paper	Type	Exchangeable cation	Modifier loading[a]	CEC[b]	Platelet size (nm)[b]	Al/Mg/Fe content (%)[c]
GelWhite GP®	GP	MMT	Ca^{++}, Na^+	0%	90–92	>100[d]	14.7/3.2/0.8
TSPP–GP	PGP	MMT	Ca^{++}, Na^+	2%	90–92	>100[d]	14.7/3.2/0.8
Cloisite® Na^+	CL	MMT	Na^+	0%	92.6	75–100	19.2/2.1/4.3
TSPP–CL	PCL	MMT	Na^+	4%	92.6	75–100	19.2/2.1/4.3
Laponite® RD	RD	Hectorite	Na^+	0%	~60	25	0/27.5/0
Laponite® RDS	RDS	Hectorite	Na^+	8.24%	~60	25	0/26/0
Laponite® B	B	Fluorohectorite	Na^+	0%	~60	25	0/27/0
Laponite® S	S	Fluorohectorite	Na^+	6.18%	~60	25	0/25/0
Laponite® JS	JS	Fluorohectorite	Na^+	10.12%	~60	25	0/22.2/0
Somasif ME100	ME	Fluorohectorite	Na^+	0%	120	100/600[d]	0/25.6/0
TSPP–ME100	PME	Fluorohectorite	Na^+	1%	120	As above	As above

[a] TSPP—tetrasodium pyrophosphate, used to render clay slurry sol properties.
[b] The values of CEC and average platelet size are from the clay provider, CEC is in the units of mequiv./100 g of clay.
[c] The values reported here are the content (%) of Al_2O_3, MgO, and Fe_2O_3 in clay from clay provider.
[d] These values were obtained from TEM results. 100/600 means the platelet dimensions are roughly 100 nm in width and 600 nm in length (see Ref. [2d]).

Hi-Res TGA 2950 thermograimetic analyzer (TA instruments) ranging from 25 to 800 °C at a heating rate of 20 °C/min. Molecular weight analysis was performed by gel permeation chromatography (GPC) using a Waters 510 pump, guard column, Waters HR2 and HR4 styragel columns, a Waters 410 differential refractometer and a Viscotek T60A dual light scattering and viscosity detector. The eluent was THF and flow rate was 1.0 ml/min. M_w and M_n were determined using universal calibration with polystyrene standard.

2.3. Preparation of cationic PMMA latex

A typical emulsion polymerization recipe is as follows. Into a four-necked 4 L Pyrex reaction kettle, which was equipped with a mechanical stirrer, argon inlet, thermometer and refluxing condenser, were placed 3000 ml of deionized water, 600 g of purified MMA, 3 g of CTABr, and 6 g of V-50. The reaction contents were purged with argon for 45 min while stirring at 300 rpm followed by heating at 70 °C for 6 h. The polymerization was stopped by cooling the reaction to room temperature and some latex was taken out for monomer conversion to be determined by a gravimetric method. For molecular weight analysis, the emulsion latex was deemulsified by freezing following by filtration and through wash with deionized water. The weight average molecular weight (M_w) and polydispersity index (PDI) were 1,079,000 and 2.48, respectively.

2.4. Peptization of clay and coagulation of PMMA latex with TSPP

The modification of clays with TSPP was carried out by adding aqueous clay slurry into a dilute TSPP water solution. The weight ratios of clay/TSPP for GP, CL, and ME are 100/4, 100/2, and 100/1, respectively. The effect of TSPP on PMMA latex stability was studied by visual inspection of the mixture of TSPP and PMMA latex in a test tube.

2.5. Heterocoagulation

Before the heterocoagulation process, a 1% (w/w) clay slurry was prepared by suspending clay in water with rigorous stirring overnight. A predetermined amount of cationic latex and clay slurry were mixed together in a beaker while stirring. The mixture was stirred for 3 h and then allowed to stand overnight. The colloid mixture was deemulsified by freezing at −20 °C; after thawing to room temperature, the mixture was filtered and thoroughly washed with water. The nanocomposite was collected and dried at 70 °C in vacuo until constant weight.

2.6. Melt extrusion and solution casting

Melt extrusion of the nanocomposites was carried out on a twin-screw MiniLab-Micro Rheology Compounder (MiniLab Rheomex CTW5, Thermo Haake, USA) at 200 °C. The extruded samples were used directly for TEM experiments and ground into fine powder for WAXD experiments. In solution cast experiments, the nanocomposite was dissolved in THF and cast into a Teflon mold, which was covered and allowed to stand for 48 h at ambient conditions. After the film was annealed at 50 °C for 12 h, the temperature was raised to 100 °C and the film was further annealed for another 12 h. A small piece of film was embedded in a 'Epo-Fix' epoxy resin for TEM experiments.

3. Results and discussion

In Table 1, we summarize the basic information about the smectites used in this study. In the present study, we have attempted to establish the influence of clay elemental composition on nancomposite thermal stability and of clay type (structure and dimension) on nanocomposite morphology. The difference between MMTs and (fluoro)hectorites is that the hectorite possess a trioctohedral structure in which the metal is solely magnesium. In MMT the octahedral layer is a dioctahedral structure, where the metal is mainly aluminum with variable amounts of iron and magnesium. The difference between Laponite® and Somasif® ME100 (both are (fluoro)hectorites) is their dimensions: Laponite® (fluoro)hectorites have an average diameter of about 25 nm and the lateral dimensions of Somasif® ME-100 are roughly 100 nm in width and 600 nm in length based on the TEM images [2d].

3.1. Effect of clay type on morphology of PMMA–clay nanocomposites

3.1.1. WAXD characterization of PMMA–smectite nanocomposites

Fig. 1 shows the WAXD patterns of nanocomposites of PMMA with GP, PGP, CL, and PCL. From Fig. 1(a), it can be seen that for all PMMA–GP nanocomposites, no feature peak was detected which suggests the formation of an exfoliated (delaminated)/disordered morphology. In Fig. 1(c) (PMMA–CL nanocomposites), a weak, broad peak centered at $2\theta = 5.4°$ (which corresponds to a basal spacing of 1.64 nm, higher than that of dried pristine CL, 0.95 nm) appeared when CL loading reached 3.67%, which is an indication of some intercalated structure. For both GP and CL, the modification with TSPP does not show any improvement in exfoliated morphology formation; on the contrary, at higher clay loadings, the modification with TSPP seems to produce increased intercalated structure (see Fig. 1(b) and (d)).

Figs. 2 and 3 give the WAXD plots of PMMA with synthetic hectorites RD, RDS and fluorohectorites B, S, and JS. It's obvious that in all of these nanocomposites exfoliated morphologies were formed with clay loadings less than 5%, regardless of clay type. Interestingly, TSSP

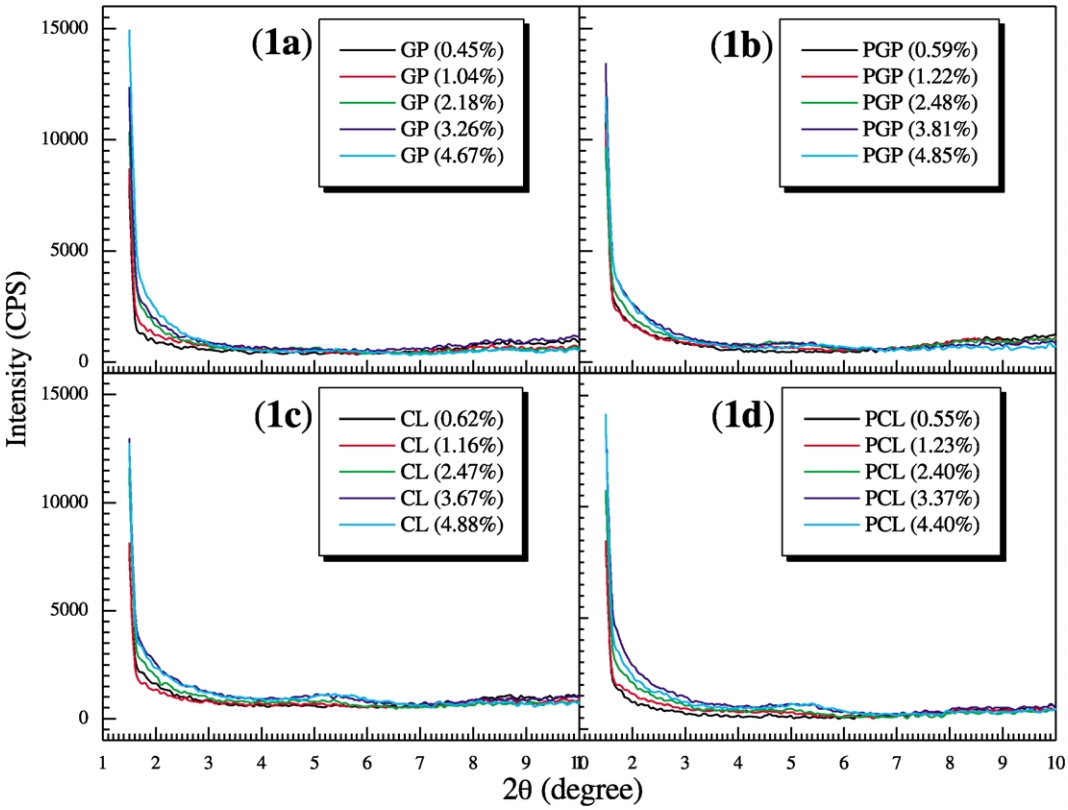

Fig. 1. WAXD patterns of PMMA nanocomposites with GP, PGP, CL and PCL.

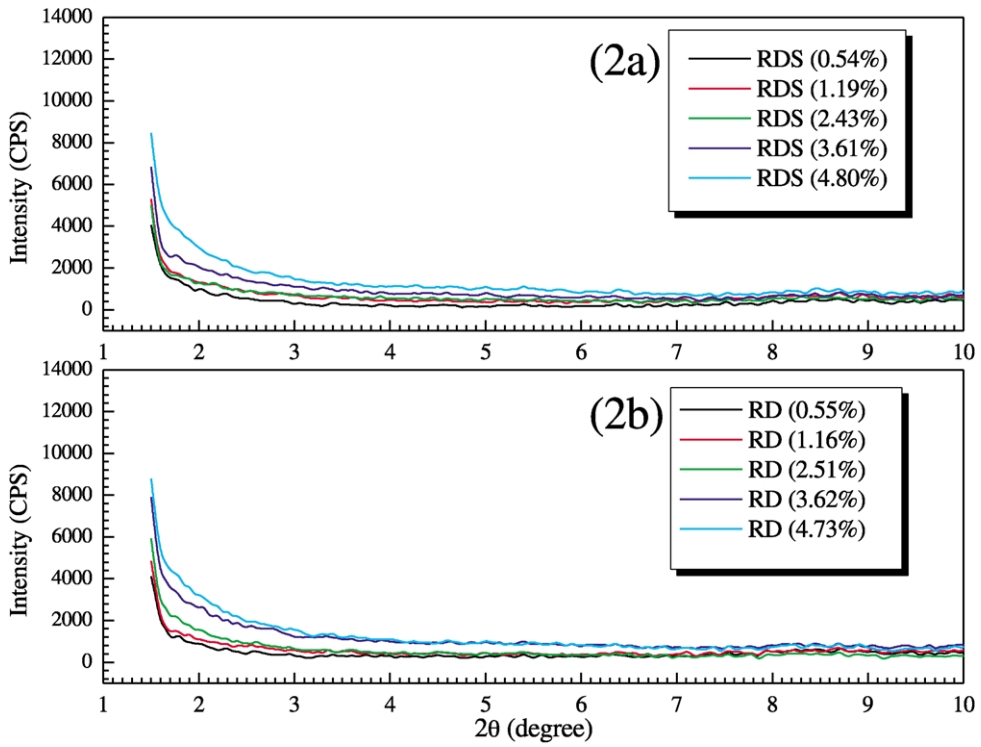

Fig. 2. WAXD patterns of PMMA nanocomposites with hectorites RD and RDS.

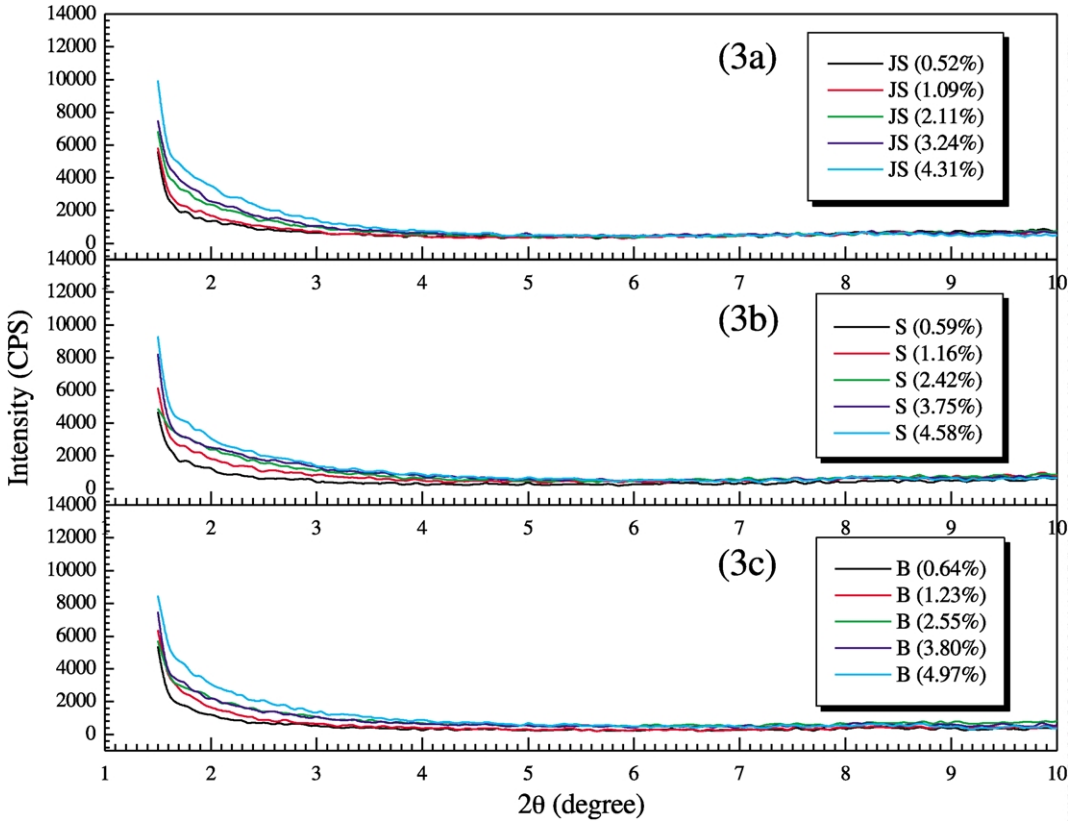

Fig. 3. WAXD patterns of PMMA nanocomposites with fluorohectorites B, S, and JS.

does not seem to affect the morphology of the nanocomposites, even though the TSPP contents in RDS, S, and JS (see Table 1) are much higher than PGP and PCL. This is contrary to what we observed in PMMA–MMT systems.

It was reported that in PLSNs, the barrier properties are related to the dimension of the clay platelets; the higher the aspect ratio of clay, the lower the permeability coefficient of the resulting nanocomposites [11]. It's also believed that the thermal stability improvement of PLSNs benefits from barrier properties [2a–c,10a]. Thus we used another synthetic fluorohectorite, Somasif® ME100, which has an aspect ratio of about 600 (much higher than the aspect ratio of 25 for the Laponite® series) to examine the relationship between thermal stability improvement and clay platelet dimensions.

The WAXD results from PMMA–ME and PMMA–PME are shown in Fig. 4. In contrast to the PMMA–Laponite® series, there is a broad peak centered at $2\theta = 6.2°$ (a basal spacing of 1.43 nm, higher than the 0.95 nm spacing for pristine Somasif® ME100) when the ME loading reaches 3.24%, indicating the presence of intercalated structures. Once again, the modification with TSPP does not affect exfoliation in the nanocomposites.

3.1.2. The heterocoagulation process and morphology development

The heterocoagulation method has been successfully used in the synthesis of inorganic/organic and organic/organic (nano)composites with well-controlled structures, through electrostatic interactions [8]. There are some reports about the use of heterocoagulation method in preparing rubber (natural and synthetic) and clay nanocomposites. However, due to the anionic property of those latexes, only intercalated structures were observed [9]. When the surface charge was cationic, which is opposite to the anionic charge of the clay surface, exfoliated structures were obtained [6c]. The key factors that determine the morphology of the resulting nanocomposite include surface charge, ζ-potential of the two colloidal particles, particle size and particle number ratio (PNR) of the two emulsions. In the cationic latex–clay colloid system, the situation becomes even more complicated due to the instability of clay colloid. The presence of most inorganic salts (e.g. NaCl, $CaCl_2$ and $AlCl_3$), alcohols, organic and polymeric cations will cause the coagulation of clay colloids while some special inorganic salts, such as TSPP, will greatly increase the stability of the clay colloid [12]. The addition of electrolyte also causes the coagulation of emulsion particles.

Clay platelets may homocoagulate during the heterocoagulation process due to the cation exchange with free surfactants which increases the NaCl concentration. In total, three competitive processes during polymer latex–clay colloid heterocoagulation may exist: cationic exchange reactions between latex/clay platelets (heterocoagulation), the homo-coagulation between clay platelets, and the homocoagulation between cationic latex particles. To

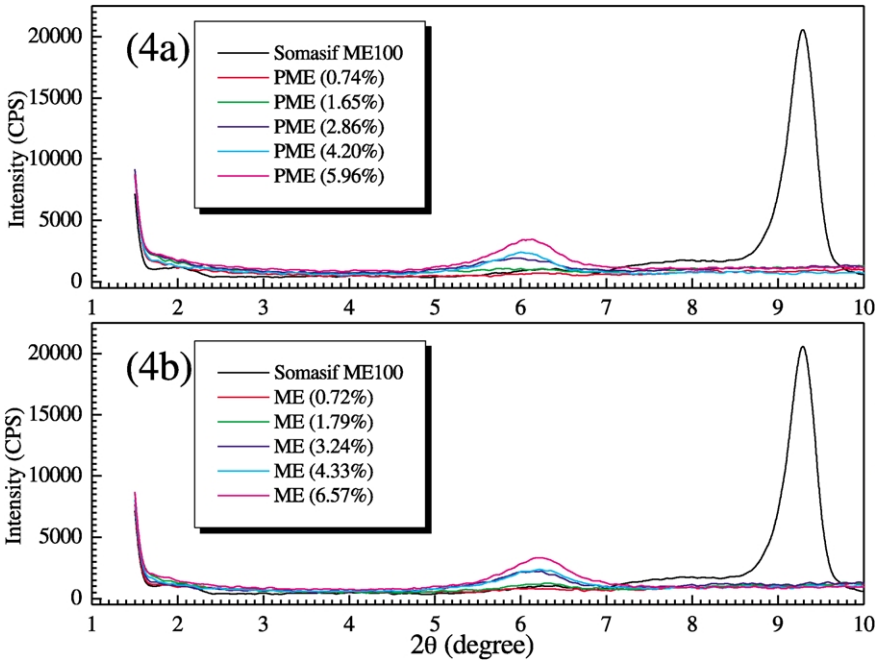

Fig. 4. WAXD patterns of PMMA with fluorohectorites ME and PME.

get exfoliated nanocomposites, the clay colloids should remain stable long enough to allow complete hetero-coagulation.

We determined the relative stability of these smectite colloids by visual inspection of the behavior of 0.05% smectite aqueous dispersions after addition of NaCl solution (test-tube tests) [12a]. The stability decreases in the order as: JS > S ≈ RDS > RD > B > GP > CL > ME100. This suggests that during the heterocoagulation process, ME100 and CL platelets more easily homocoagulate due to the NaCl produced by cation exchange reactions, especially at higher clay loadings.

The same tests of the smectites modified with TSPP showed an increase in the colloidal stability, which is in good agreement with previous reports [12]. Because the modification with TSPP increases the clay colloidal stability, it is puzzling that there is no increase in exfoliation for the GPG, PCL and PME systems. Better smectite colloidal stability should improve chances for latex–clay cation exchange reactions and hence lead to a higher degree of exfoliation. To answer this question, we checked the effect of TSPP on the stability of PMMA latex. We found that when TSPP reached 0.06 wt% with respect to PMMA, coagulation of the latex occurred. This suggests that TSPP may play dual roles by increasing the stability of smectite colloids and acting as a coagulant for the polymer latex. The coagulation of polymer latex and release of NaCl during this process may be the reason for no improvement in exfoliation and perhaps additional intercalation. We do not understand the lack of TSPP influence in the Laponite® series; especially in light of the higher TSPP loadings (6.18–10.12%) relative to MMT systems.

The morphology differences may also relate to the size differences between those smectite platelets. In an experiment containing two smectites, it was found that the larger particles are selectively coagulated [13]. Thus, the fully exfoliated structures in the Laponite® series may be due to their smaller size.

3.1.3. TEM characterization and the heterocoagulation model

Scheme 1 depicts the possible morphologies of PLSNs in the heterocoagulation process. Different heterocoagulation/homocoagulation processes may lead to exfoliated (a, b, and c), mixed (d) and intercalated (e) structures depending on relative particle sizes and the particle number ratio (PNR).

Fig. 5(a) is a typical TEM image of PMMA–GP nanocomposites (4.67%) at low magnification, while Fig. 5(b) is the image of the same sample at higher magnification. From Fig. 5(a) it can be concluded that the clay platelets are macroscopically dispersed. From Fig. 5(b), we speculate that single platelets are situated between polymer particles which may correspond to 'Model a' in Scheme 1. In combination with the WAXD results in Fig. 1, we conclude that PMMA–GP nanocomposites with fully exfoliated morphologies were obtained by the heterocoagulation method.

Fig. 6(a) is the TEM pattern of PMMA–CL (4.88%) nanocomposite. Co-existing exfoliated and intercalated structures are observed which corresponds with the WAXD results. In this case, the heterocoagulation process may correspond to 'Model d' in Scheme 1. Consistent with the small diameter of the Laponite® clay relative to the polymer particles (typical diameter of the polymer particles is about 1209 nm), the TEM image of PMMA–RDS

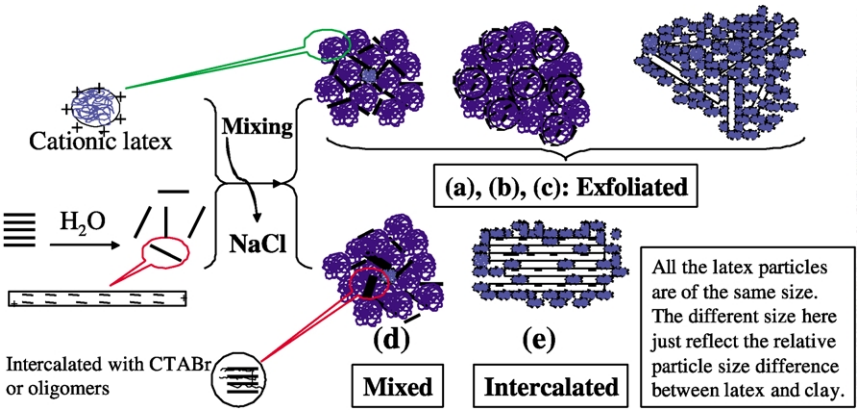

Scheme 1. Possible morphologies formed during heterocoagulaiton process.

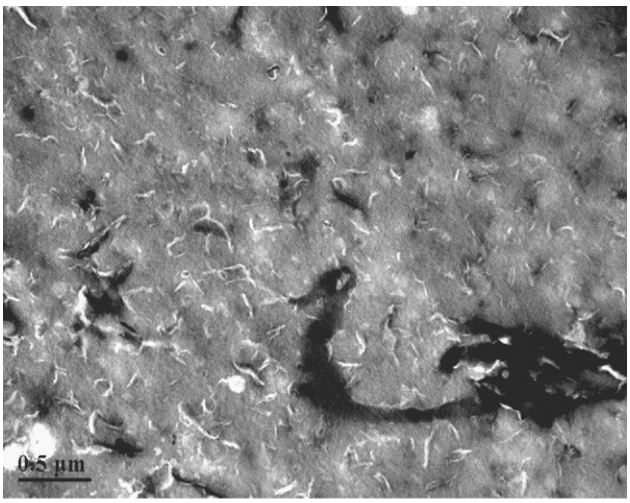

Fig. 5. (a) Low magnification TEM image of PMMA–GP (4.67%) nanocomposite. (b) High magnification TEM image of PMMA–GP (4.67%) nanocomposite.

(4.80%) nanocomposite shown in Fig. 6(b) suggests heterocoagulation via 'Model b' in Scheme 1. Fig. 6(c) shows the TEM result from PMMA–ME nanocomposite at 2.86% ME loading. During the heterocoagulation process, intercalation is predominant and results in the dispersion of clay stacks in the PMMA matrix, which probably corresponds to 'Model e' in Scheme 1.

One important issue in PLSNs is that whether the morphology can be preserved during processing. Fig. 7(a) and (b) show the typical TEM images of nanocomposites after melt extrusion and solution casting. In accord with WAXD results, the nanocomposites preserved their exfoliation morphology after processing. These results suggest that during the heterocoagulation process, the cation exchange reactions between Na^+ and PMMA end groups did occur, otherwise the miscibility of PMMA with clay or CTABr modified clay (due to the cation exchange reaction) would be poor and phase separation would likely occur during solution casting or melt extrusion.

3.2. Effect of clay type on thermal stability of PMMA–clay nanocomposites

Fig. 8(a)–(c) summarize the thermal degradation behaviors of PMMA–clay nanocomposites. Derivative thermogravimetry analysis (DTG) was used to study the thermal degradation rates of all PMMA–clay nanocomposites in this study. From Fig. 8 we can see that there are two peak decomposition rates during PMMA degradation at 280 and 322 °C. Fig. 8(a) displays the DTG patterns of PMMA–GP, PGP, CL and PCL in air atmosphere. Even at 0.5% clay loading, the decomposition shifted to higher temperatures with the major decomposition observed at 348 °C. In the PMMA–CL nanocomposites, the first peak significantly diminished when the clay loading reached 3.67%, beyond which there is no further improvement in thermal stability. In the PMMA–GP nanocomposites, the largest decrease in the lower temperature process occurred at 4.67% loading.

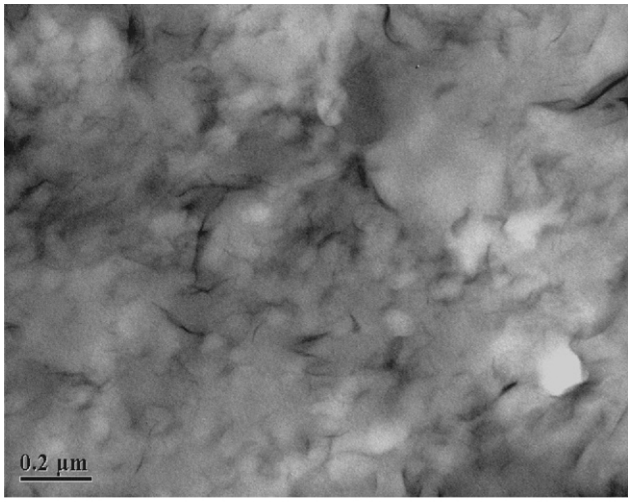

(a)

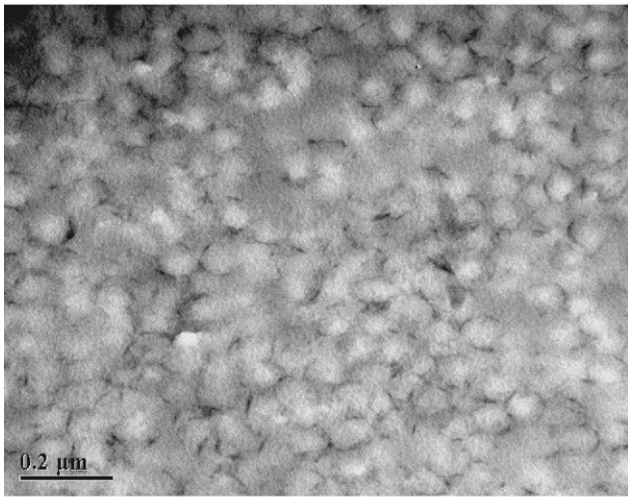

(b)

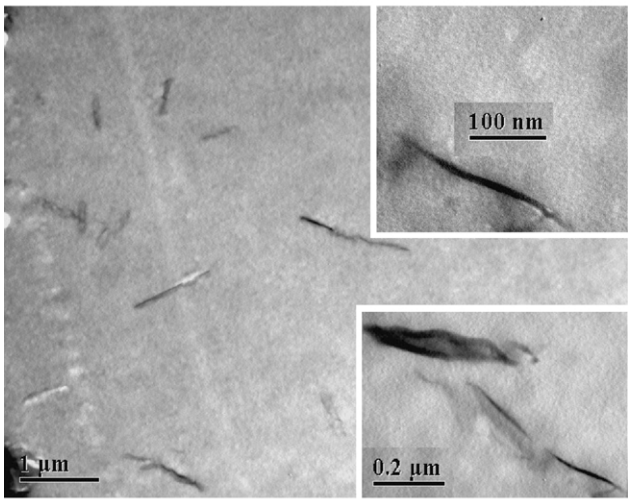

(c)

Fig. 6. (a) TEM image of PMMA–CL (4.88%) nanocomposite. (b) TEM image of PMMA–RDS (4.80%) nanocomposite. (c) TEM image of PMMA–ME (2.86%) nanocomposite.

Comparing the DTG curves of PMMA–GP and PMMA–CL nanocomposites, CL is more efficient in reducing the lower temperature decomposition and the higher temperature process increased by 10 °C. At lower clay loadings, TSPP seems to have a synergetic effect with GP and CL, but with an increase of clay loading, this effect disappeared. Fig. 8(b) shows the thermal decomposition behavior of PMMA nanocomposites from the Laponite® series of (fluoro)hectorites. Small improvements in thermal stability were observed when the hectorite loadings reached 2.5%, but the change at 4.0% loading is lower than the PMMA–MMT systems with a loading of 0.5%. At low hectorite loadings, the thermal stability of the nanocomposites is lower than PMMA. In this system, the presence of TSSP showed no effect on thermal stability, which is different from that in PMMA–MMT system. The presence of Somasif® ME100 in PMMA (Fig. 8(c)) decreased the onset temperature of thermal degradation. All the DTG curves are the same, regardless of clay loadings and the presence of TSPP.

It is generally accepted that the decomposition of radically polymerized PMMA in nitrogen atmosphere consists of three stages: the first (100–200 °C) is ascribed to the weak head–head linkages in the main chain; the second (200–300 °C) is terminal vinyl group decomposition; and the third (300–400 °C) is due to the random scission of polymer main chain [14]. While decomposing in the presence of oxygen, the first peak disappears and the second peak either merges with the third peak or becomes a shoulder to the third peak depending on the heating rate. This phenomenon was explained by the dual function of oxygen in PMMA decomposition. At lower temperatures, oxygen inhibits PMMA decomposition by reacting with a polymeric radical and forming a more stable new polymeric radical. At temperatures above 270 °C, this new polymeric radical decomposes and releases a more reactive radical resulting in the acceleration of PMMA decomposition [15]. The improvement of the thermal stability in PMMA nanocomposites and the different behaviors of different types of smectites may be associated with reactivity of different metals with polymeric radicals and the different thermal stability of the resulting complexes or coordinates.

Clays can act as free radical scavengers and traps by reacting with the propagating or initiating radicals [16]. Giannelis and co-workers [10b] reported that PMMA–MMT nanocomposites possess better thermal stability than those from fluorohectorite and he attributed this to the higher amount of aluminosilicates in MMT. Zhu et al. [10c] proposed an effect of iron on PS nanocomposite thermal stability improvement. Gilman et al. [10a] suggested that intercalated nanocomposites may show better thermal stability than the exfoliated counterparts. Considering our DTG results in Fig. 8, we think that both iron and aluminum can improve the thermal stability of PMMA in

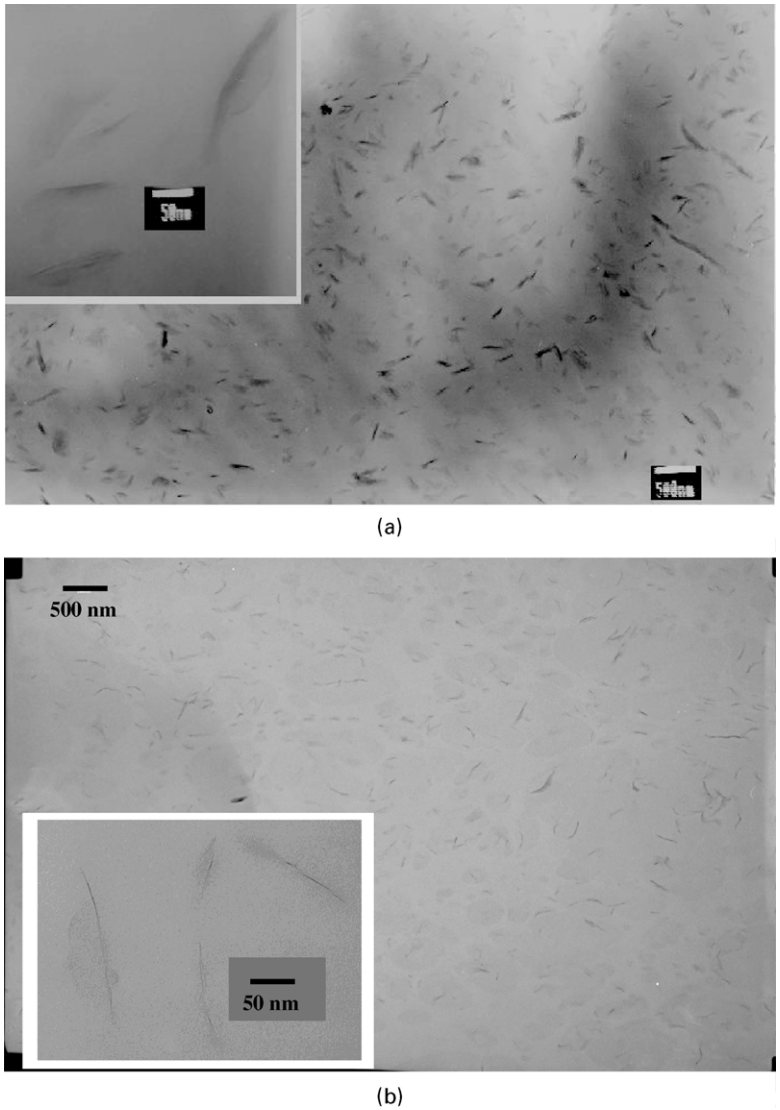

Fig. 7. (a) TEM image of PMMA–CL (2.47%) nanocomposite after melt extrusion. (b) TEM image of PMMA–GP (4.67%) nanocomposite after solution casting.

nanocomposites, but iron is much more effective than aluminum. The effect of magnesium on thermal stability improvement is very small or nil. By comparing the DTG results from exfoliated nanocomposites of PMMA–ME with those of PMMA–Laponite®, we didn't observe any effect of particle size on thermal stability improvement.

4. Summary

In this paper we showed that heterocoagulation is a useful method to prepare PLSNs. Clay platelet dimensions and colloidal stability have a significant effect on the nanocomposite morphology. PMMA nanocomposites from GelWhite GP® and Laponite® have fully exfoliated structures up to 5% clay loading. For Cloisite® Na^+ and Somasif® ME100, the morphologies depend on clay loadings. Although the modification of clay with tetrasodium pyrophosphate improves its colloidal stability, such modification doesn't enhance exfoliation. Exfoliated PMMA nanocomposites of GelWhite GP® and Cloisite® Na^+ prepared by heterocoagulation method showed good morphology preservation during solution and melt processing. Both iron and aluminum contribute to the improvement of thermal stability of PMMA nanocomposites, but iron is more effective. Although it was assumed that the improvement of PLSNs' thermal stability partially results from the barrier properties, we didn't observe a dependence of thermal stability on clay dimension.

Acknowledgements

This research was supported by the DURINT on

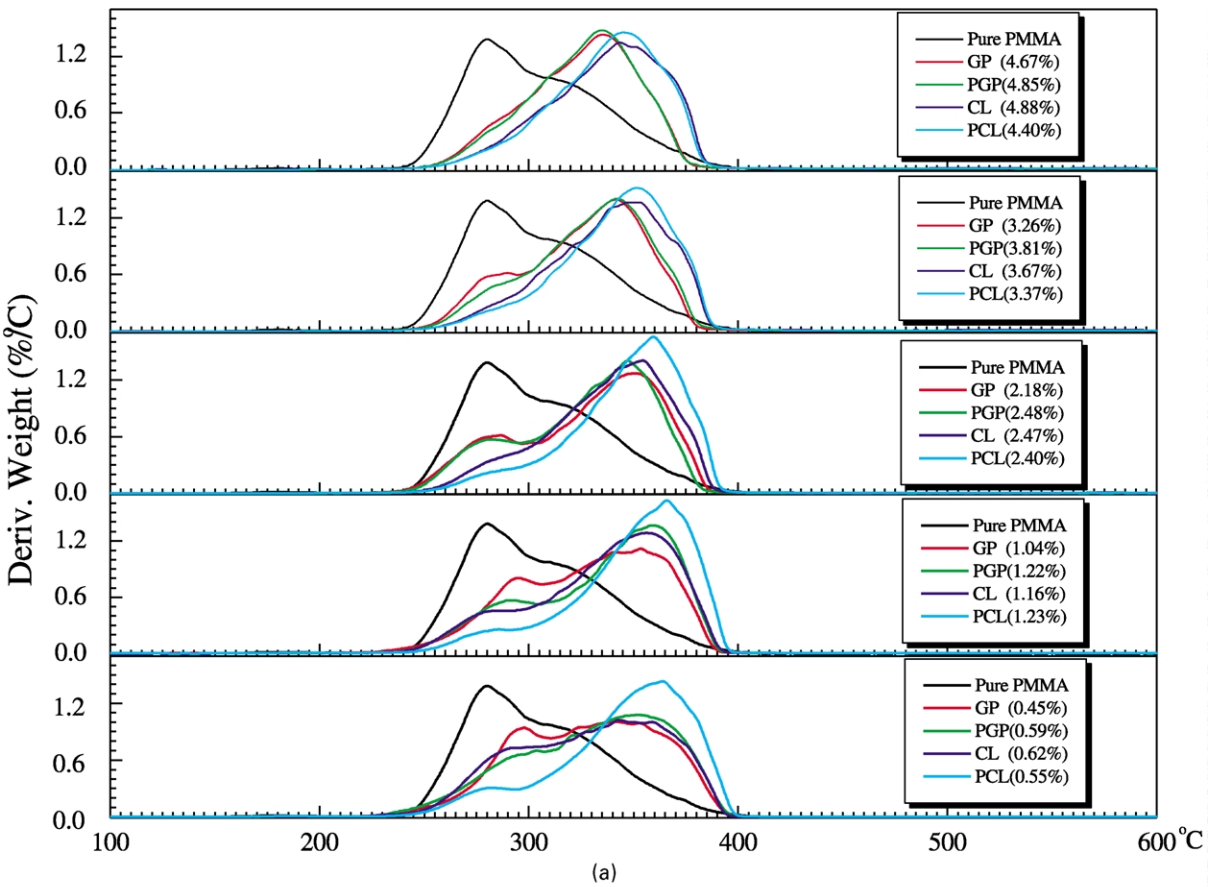
Deriv. Weight (%/°C)
Pure PMMA
GP (4.67%)
PGP(4.85%)
CL (4.88%)
PCL(4.40%)
Pure PMMA
GP (3.26%)
PGP(3.81%)
CL (3.67%)
PCL(3.37%)
Pure PMMA
GP (2.18%)
PGP(2.48%)
CL (2.47%)
PCL(2.40%)
Pure PMMA
GP (1.04%)
PGP(1.22%)
CL (1.16%)
PCL(1.23%)
Pure PMMA
GP (0.45%)
PGP(0.59%)
CL (0.62%)
PCL(0.55%)
100
200
300
400
500
600 °C

(a)

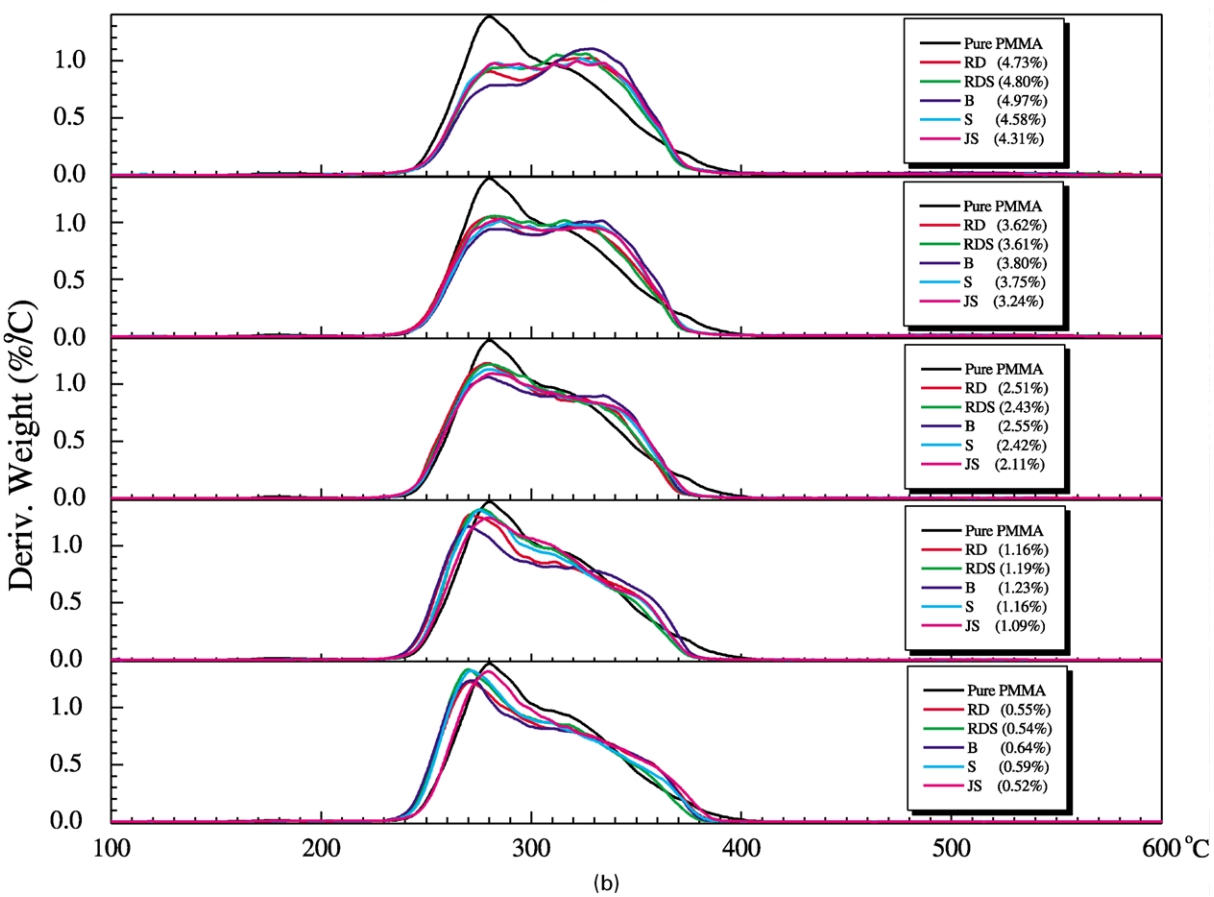
Deriv. Weight (%/°C)
Pure PMMA
RD (4.73%)
RDS (4.80%)
B (4.97%)
S (4.58%)
JS (4.31%)
Pure PMMA
RD (3.62%)
RDS (3.61%)
B (3.80%)
S (3.75%)
JS (3.24%)
Pure PMMA
RD (2.51%)
RDS (2.43%)
B (2.55%)
S (2.42%)
JS (2.11%)
Pure PMMA
RD (1.16%)
RDS (1.19%)
B (1.23%)
S (1.16%)
JS (1.09%)
Pure PMMA
RD (0.55%)
RDS (0.54%)
B (0.64%)
S (0.59%)
JS (0.52%)
100
200
300
400
500
600 °C

(b)

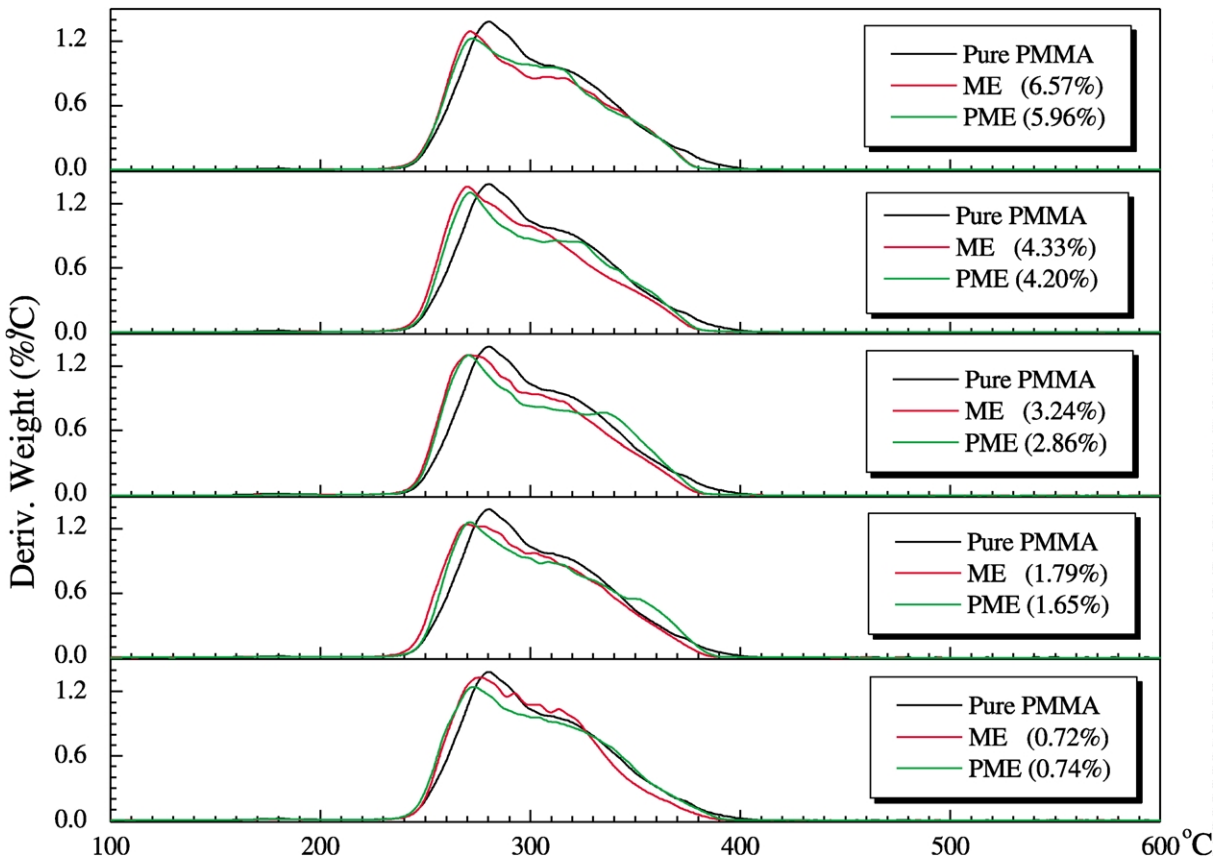

Fig. 8 (*continued*)

Fig. 8. (a). DTG comparison of PMMA–MMT nanocomposites (GP, PGP, CL and PCL) at different clay loadings. (b) DTG comparison of PMMA–(fluoro)hectorites nanocomposites (RD, RDS, B, S and JS) at different clay loadings. (c) DTG comparison of PMMA–fluorohectorite nanocomposites (ME at different clay loadings.

Microstructure, Processing and Mechanical Performance of Polymer Nanocomposites, Air Force Contract No. F49620-01-1-0447. The authors thank Professor Stephen Z.D. Cheng for access to a wide angle X-ray diffractometer.

References

[1] (a) Usuki A, Kojima Y, Kawasumi M, Okada A, Kurauchi T, Kamigaito O. J Mater Res 1993;8(5):1174–8. (b) Usuki A, Kojima Y, Kawasumi M, Okada A, Kurauchi T, Fukushima Y, Kamigaito O. J Mater Res 1993;8(5):1179–84. (c) Kojima Y, Usuki A, Kawasumi M, Okada A, Fukushima Y, Kurauchi T, Kamigaito O. J Mater Res 1993;8(5):1185–9.

[2] For recent reviews on preparation and properties of polymer–clay nanocomposites, see: (a)Giannelis EP. Adv Mater 1996;8(1):29–35. (b) Alexandre M, Dubois P. Mater Sci Engng 2000;28(1/2):1–63. (c) Pinnavaia TJ, Beall GW. Polymer–clay nanocomposites. New York: Wiley; 2000. (d) Zilg C, Dietsche F, Hoffman B, Dietrich C, Mulhaupt R. Macromol Symp 2001;169(1):65–77. (e) Vaia RA, Giannelis EP. MRS bulletin; 2001 May. p. 394–401. (f) Schmidt D, Shah D, Giannelis EP. Curr Opin Solid State Mater Sci 2002;6(3):205–12.

[3] (a) Gao Z, Xie W, Hwu JM, Wells L, Pan W-P. J Therm Anal Cal 2001;64(2):467–75. (b) Yeh J-M, Liou S-H, Lin C-Y, Cheng C-Y, Chang Y-W. Chem Mater 2002;14(1):154–61.

[4] (a) Shen Z, Simon GP, Cheng Y-B. Mater Res Soc Symp Proc 1999; 576:137–42. (b) Fischer HR, Gielgens LH, Koster TPM. Acta Polym 1999;50(4):122–6. (c) Zilg C, Thomann R, Baumert M, Finter J, Mulhaupt R. Macromol Rapid Commun 2000;21(17):1214–9. (d) Lee H, Hsieh AJ, McKinley GH. Polym Mater Sci Engng 2002;87:19–20.

[5] (a) Biasci L, Aglietto M, Ruggeri G, Ciardelli F. Polymer 1994; 35(15):3296–304. (b) Chen G, Chen X, Lin Z, Ye W. J Mater Sci Lett 1999;18(21):1761–3. (c) Dietsche F, Mulhaupt R. Polym Bull 1999; 43(4/5):395–402. (d) Okamoto M, Morita S, Taguchi H, Kim YH, Kataka T, Tateyama H. Polymer 2000;41(10):3887–90. (e) Dietsche F, Thomann Y, Thomann F, Mulhaupt R. J Appl Polym Sci 2000; 75(3):396–405. (f) Zeng C, Lee LJ. Macromolecules 2001;34(12): 4098–103. (g) Bottcher H, Hallensleben ML, Nuß S, Wurm H, Bauer J, Behrens P. J Mater Chem 2002;12(5):1351–4. (h) Zhu J, Start P, Mauritz KA, Wilkie GA. Polym Degrad Stab 2002;77(2):253–8. (i) Wang D, Zhu J, Yao Q, Wilkie GA. Chem Mater 2002;14(9): 3837–43. (j) Su S, Wilkie CA. J Polym Sci, Part A: Polym Chem 2003;41(8):1124–35. (k) Zhang W, Li Y, Wei L, Fang YE. Mater Lett 2003;57(22–23):3366–70.

[6] (a) Lee DC, Jang LW. J Appl Polym Sci 1996;61(7):1117–22. (b) Bandyopadhyay S, Giannelis EP, Hsieh AJ. Polym Mater Sci Engng 2000;82:19–20. (c) Huang X, Brittain WJ. Macromolecules 2001; 34(10):3255–60. (d) Choi YS, Choi MH, Wang KH, Kim SO, Kim YK, Chung IJ. Macromolecules 2001;34(26):8978–85.

[7] Brittain WJ. In preparation.

[8] (a) Furusawa K. In: Esumi K, editor. Polymer interfaces and

emulsions. New York: Marcel Dekker; 1999. p. 219. (b) Maroto JA, de las Nieves FJ. J Colloid Surf A 1995;96(1/2):121–33. (c) Islam AM, Chowdhry BZ, Snowden MJ. Adv Colloid Interface Sci 1995; 62(2/3):109–36. (d) Lagaly G, Mecking O, Penner D. Colloid Polym Sci 2001;279(11):1090–6. (e) Lagaly G, Mecking O, Penner D. Colloid Polym Sci 2001;279(11):1097–103. (f) Rossi GB, Beaucage G, Dang TD, Vaia RA. Nano Lett 2002;2(4):319–23. (g) Yamaguchi K, Ito M, Taniguchi T, Kawaguchi S, Nagai K. Chem Lett 2002; 31(12):1188–9. (h) Pham HH, Kumacheva E. Macromol Symp 2003; 192(1):191–206.

[9] (a) Karger Kocsis J, Varghese S. Polymer 2003;44(17):4921–7. (b) Wang Y, Zhang L, Tang C, Yu DS. J Appl Polym Sci 2000;78(11): 1879–83. (c) Wu YP, Zhang LQ, Wang YQ, Liang Y, Yu DS. J Appl Polym Sci 2001;82(11):2842–8.

[10] (a) Gilman JW. Appl Clay Sci 1999;15(1/2):31–49. (b) Bandyopadhyay S, Giannelis EP. Polym Mater Sci Engng 2000;82:208–10. (c) Zhu J, Uhl FM, Morgan AB, Wilkie CA. Chem Mater 2001;13(12):4649–54.

[11] Yano K, Usuki A, Okada A. J Polym Sci, Part A: Polym Chem 1997; 35(11):2289–94.

[12] (a) Van Olphen H. Clay colloid chemistry, 2nd ed. New York: Wiley; 1977. (b) Lagaly G, Ziesmer S. Adv Colloid Interface Sci 2003; 100–2. also p. 105–128.

[13] Lagaly G. In: Dobias B, editor. Coagulation and flocculation theory and applications. Surfactant science series, vol. 47. New York: Marcel Dekker; 1993. p. 427.

[14] (a) Hirata T, Kashiwagi T, Brown JE. Macromolecules 1985;18(7): 1410–8. (b) Kashiwagi T, Inaba A, Brown JE, Hatada K, Kitayama T, Masuda E. Macromolecules 1986;19(8):2160–8. (c) Manring LE. Macromolecules 1989;22(6):2673–7. (d) Manring LE, Sogah DY, Cohen GM. Macromolecules 1989;22(12):4652–4. (e) Holland BJ, Hay JN. Polym Degrad Stab 2002;77(3):435–9.

[15] Peterson JD, Vyazovkin S, Wight CA. J Phys Chem B 1999;103(38): 8087–92.

[16] Solomon DH, Swift JD. J Appl Polym Sci 1967;11(12):2567–75.